HHS Public Access

Author manuscript

Nat Biomed Eng. Author manuscript; available in PMC 2024 May 15.

Published in final edited form as:

Nat Biomed Eng. 2020 May ; 4(5): 531–543. doi:10.1038/s41551-020-0549-2.

Collagen-binding IL-12 enhances tumour inflammation and drives the complete remission of established 'immunologically cold' murine tumours

Aslan Mansurov[1,&], **Jun Ishihara**[1,&,*], **Peyman Hosseinchi**[1], **Lambert Potin**[1], **Tiffany M. Marchell**[1,2], **Ako Ishihara**[1], **John-Michael Williford**[1], **Aaron T. Alpar**[1], **Michal M. Raczy**[1], **Laura T. Gray**[1], **Melody A. Swartz**[1,2,3], **Jeffrey A. Hubbell**[1,2,*]

[1]Pritzker School of Molecular Engineering, University of Chicago, Chicago, IL, 60637, USA

[2]Committee on Immunology, University of Chicago, Chicago, IL, 60637, USA

[3]Ben May Department for Cancer Research, University of Chicago, Chicago, IL, 60637, USA

Abstract

Checkpoint inhibitor (CPI) immunotherapy has achieved remarkable clinical success, yet its efficacy in 'immunologically cold' tumours has been modest. Interleukin (IL)-12 is a powerful cytokine that activates the innate and adaptive arms of the immune system, yet its administration has been associated with immune-related adverse events. Here, we show that the intravenous administration of a collagen-binding domain fused to IL-12 (CBD–IL-12) in mice bearing aggressive murine tumours accumulates in the tumour stroma, owing to exposed collagen in the disordered tumour vasculature. In comparison with the administration of unmodified IL-12, CBD–IL-12 induced sustained intratumoral levels of interferon-γ, markedly reduced its systemic levels as well as organ damage, and led to superior anticancer efficacy, eliciting complete regression of CPI-unresponsive breast tumours. Furthermore, CBD–IL-12 potently synergized with CPI to eradicate large established melanoma, induced antigen-specific immunological memory, and controlled tumour growth in a genetically engineered mouse model of melanoma. CBD–IL-12 may potentiate CPI immunotherapy for immunologically cold tumours.

 Correspondence and requests for materials should be addressed to J.A.H.

*Corresponding authors, jhubbell@uchicago.edu; juni@uchicago.edu.
&These authors contributed equally

Author contributions

A.M., J.I., M.A.S and J.A.H designed the experiments and wrote the manuscript. A.M. and J.I. performed the experiments. P.H. assisted with the pulmonary metastasis model. L.P. assisted with the autochthonous melanoma model. T.M. assisted with the antigen restimulation experiment and prepared B16F10 exosomes. A.I. blindly evaluated histological sections. J.M.W. and L.T.G. assisted with tumour experiments. A.T.A. assisted with blood chemistry analysis. M.M.R. assisted with and analysed MALDI-TOF data.

Competing interests

J.I., A.I., M.A.S., J.A.H., are inventors on U.S. Provisional Patent applications 62/638,520, 28/984,351, and 62/727,156. J.I., A.I., M.A.S., J.A.H. are founders and shareholders in Arrow Immune Inc., which is developing the technology presented in this report, and M.A.S., J.A.H. have leadership roles in that company. The remaining authors declare no competing of interests.

Additional information

Supplementary information is available for this paper at https://doi.org/10.1038/s41551-01X-XXXX-X.

Immunotherapy is a promising approach for treating cancer patients. Although checkpoint inhibitor (CPI) therapies, such as anti-cytotoxic T lymphocyte antigen-4 (α-CTLA-4) and anti-programmed death-1 (α-PD-1) antibodies, have achieved clinical success, these antibodies fail to induce regression of established tumours in a majority of patients, keeping the complete response (CR) rates low[1]. CPI therapy inherently relies on pre-existing antitumor immunity, which is absent in poorly immunogenic, so called "cold" tumors[2]. To trigger immunologic destruction of advanced, cold tumours, sufficient numbers of effector immune cells capable of recognizing tumour antigens with high avidity must infiltrate the tumour stroma[3]. A strategy that aims to convert immune-excluded tumours into immune-infiltrated tumours would be a major advancement in cancer care.

Interleukin (IL)-12 is considered to be an attractive antitumor therapeutic cytokine as it can activate both the innate and the adaptive arms of the immune system[4], and is able to elicit antigen-specific immune responses[5, 6]. IL-12 promotes Th1 polarization, results in interferon-γ (IFNγ) secretion by effector cells such as $CD8^+$ T cells[7], and stimulates antigen presentation[8]. Despite encouraging preclinical findings, systemic administration of recombinant human IL-12 (rhIL-12) showed unsatisfactory outcomes in clinical trials due to intolerable immune-related adverse events (irAEs), resulting in discontinuation of trials with systemic IL-12[9]. A major barrier in recombinant IL-12 therapy stems from the inability to reach sufficiently high local concentrations within the tumour microenvironment (TME)[10], thus motivating the development of tumour-targeted IL-12 therapy to unleash the full therapeutic potential of this cytokine. In this regard, IL-12 has recently been fused with lumican, a collagen-binding protein, which can be retained within the tumour matrix upon intratumoral injection[11]. An approach that would enable intravenous (i.v.) administration could further extend the translatability of IL-12 therapy to non-superficial and metastatic tumours.

We have recently reported that the A3 collagen-binding domain (CBD) of von Willebrand factor (VWF) can be retained within solid tumours upon i.v. administration due to exposure of collagen within the tumour stroma associated with vascular leakiness[12]. Chemical conjugation of CBD protein to CPI antibodies and recombinant fusion to IL-2 resulted in enhanced antitumor efficacy compared to their unmodified forms, but the efficacy was insufficiently strong to show CRs in aggressive models such as B16F10 melanoma and the immune-excluded EMT6 mammary carcinoma. Here, we have focused our attention on a cytokine more likely to induce tumour inflammation, with the objective to make cold tumours inflamed and thus more responsive to CPI therapy, installing collagen affinity to IL-12 to enhance its efficacy and overcome safety challenges that have hindered its clinical translation.

Results

CBD-IL-12 binds to collagen I and III with high affinity

We exploited the heterodimeric structure of IL-12 and fused one CBD molecule to each of the subunits to install high affinity to collagen (Fig. 1a). CBD-IL-12 exhibited slightly reduced bioactivity compared to IL-12 as assessed by STAT4 phosphorylation (Fig. 1b) and splenocyte activation (Supplementary Fig. 1a). We further characterized the molecular

weights of IL-12 and CBD-IL-12 by SDS-polyacrylamide gel electrophoresis (SDS-PAGE) (Supplementary Fig. 1b) and matrix-assisted laser desorption/ionization time-of-flight (MALDI-TOF) spectrometry (Supplementary Fig. 1c,d). According to MALDI-TOF spectra, the molecular weights of IL-12 and CBD-IL-12 were 62.8 kDa and 106.6 kDa, respectively. We determined the equilibrium dissociation constants of CBD-IL-12 against collagen I and III using surface plasmon resonance (SPR), which were 3.6 and 6.2 nM, respectively (Fig. 1c,d). Such high binding affinity can be partially attributed to the avidity effect caused by two CBD molecules fused to IL-12, since monoCBD-IL-12 exhibited weaker binding to collagen I (Supplementary Fig. 1e). Unmodified IL-12 did not bind to collagen I, as confirmed by SPR (Supplementary Fig. 1f). CBD-IL-12, but not unmodified IL-12, bound to human melanoma cryosections and localized around the blood vessels, where collagen is particularly enriched (Fig. 1e,f). These data show that CBD-IL-12 is functional as we have designed it, capable of activating cells *in vitro* and binding to collagens I and III with high affinity.

CBD-IL-12 is more efficacious than unmodified IL-12 in melanoma and breast cancer

IL-12 has been tested clinically, both alone and in combination, in patients with advanced melanoma and breast cancer[13–15]. We first examined the antitumor activity of CBD-IL-12 in the aggressive B16F10 melanoma model (Fig. 2a,b). Mice bearing day 7 B16F10 tumours (~60 mm^3 at the start of therapy) were treated once with either PBS, IL-12 or equimolar CBD-IL-12. We administered the cytokines either peritumourally (p.t.) or i.v. to determine the most efficacious injection route. Systemic administration of CBD-IL-12 resulted in robust regression of B16F10 melanoma, as opposed to both p.t.- and i.v.-administered unmodified IL-12, which delayed the tumour growth compared to treatment with PBS. Interestingly, although p.t. injection of CBD-IL-12 was still more favourable than either route of unmodified IL-12, its antitumor efficacy was inferior to i.v. administration of CBD-IL-12. A single i.v. injection of CBD-IL-12 resulted in 10 CR out of 15 treated mice (67%). We also compared the antitumor efficacy of CBD-IL-12 to CBD-IL-2[12] and also tested lower doses of CBD-IL-12 (Supplementary Fig. 2). CBD-IL-12 showed dose-dependent antitumor efficacy and was more efficacious than equimolar CBD-IL-2.

We then tested the efficacy of CBD-IL-12 in the triple negative, immune-excluded EMT6 breast cancer model[12, 16] (Fig. 2c,d). CBD-IL-12 administered i.v. once on day 7 resulted in 13 CR out of 15 mice (87%), whereas unmodified IL-12 resulted in 6 CR out of 15 mice (40%). Importantly, CBD-IL-12-treated mice that were tumour-free developed systemic immunological memory, as 12 mice out of 13 rejected rechallenge with the EMT6 tumour cells in their contralateral mammary fat pad. These data indicate that CBD fusion to IL-12 greatly improves the antitumor responses and results in complete tumour remissions of moderately-sized B16F10 melanoma and EMT6 mammary carcinoma in the majority of mice when used as a single agent.

CBD-IL-12 demonstrates increased accumulation in tumours and decreased systemic circulation and causes profound changes in the tumour microenvironment

Recombinant CBD efficiently accumulates within tumours following i.v. administration[12]. To confirm that CBD-fused IL-12 targets the tumour, EMT6-bearing mice were injected

with fluorescently labelled IL-12 or CBD-IL-12. As expected, CBD-IL-12 had significantly greater accumulation in the tumour compared to unmodified IL-12 (Fig. 3a). In non-tumour-bearing mice, IL-12 and CBD-IL-12 had similar biodistribution, with the exception of the lung, in which IL-12 had greater accumulation (Supplementary Fig. 3a). Increasing the molecular weight of a cytokine can alter its circulation half-life, which can potentially contribute to increased toxicity[17]. CBD-IL-12 exhibited much shorter serum half-life compared to the unmodified IL-12, despite having a larger molecular weight (Fig. 3b).

EMT6 tumours are characterized by very sparse $CD8^+$ T cell infiltration[12], a property that is shared among many human immune-excluded tumour types[18]. To visualize how the tumour microenvironment is re-shaped upon treatment with CBD-IL-12, we analysed $CD8^+$ T cell frequency by immunohistochemistry (Fig. 3c). CBD-IL-12 therapy induced extensive infiltration of $CD8^+$ T cells into the EMT6 tumour stroma, converting an immunologically cold tumour into a more inflamed one.

In melanoma patients treated with rhIL-12, the ability to maintain a robust and prolonged elevation of IFNγ is associated with positive clinical response[19] and expression of IFNγ-responsive genes in the tumour predicts clinical response to immunotherapy[20]. Treatment with CBD-IL-12 but not unmodified IL-12 induced sustained levels of B16F10 intratumoral IFNγ, the main mediator of antitumor activity of IL-12, for at least 4 days following treatment (Fig. 3d). On day 4 after treatment, the amount of intratumoral IFNγ was about 4 times higher in the CBD-IL-12-treated cohort compared to equimolar IL-12 (Fig. 3e). Additionally, CBD-fused IL-12 increased intratumoral levels of various proinflammatory cytokines/chemokines, such as C-X-C motif chemokine 10 (CXCL10), a chemokine that is important for effector T cell recruitment[21] and anti-angiogenesis[22], and IL-1β, a cytokine required for priming of IFNγ-producing, antigen-specific $CD8^+$ T cells[23] (Fig. 3f–i). No differences were observed in intratumoral levels of TNFα or IL-6 (Supplementary Fig. 3b,c). We also quantified tumour-infiltrating lymphocytes and identified IFNγ-producing immune cells by *in vivo* injection of brefeldin A (BFA)[24] in B16F10 melanoma model (Supplementary Fig. 4). Treatment with CBD-IL-12 led to increases in $CD8^+$ T cell-to-Treg ratio (Supplementary Fig. 4d) and $IFN\gamma^+$ immune cells (Supplementary Fig. 4g). IFNγ-producing $CD8^+$ T cells (Supplementary Fig. 4h) constituted the majority of total IFNγ production (Supplementary Fig. 4m).

CBD fusion to IL-12 decreases systemic toxicity

One of the major hurdles in clinical translation of recombinant IL-12 therapy is the toxicity induced by this cytokine[14]. Systemic IFNγ is the main contributor to the irAEs of IL-12. Experiments with $IFN\gamma R^{-/-}$ mice revealed that most of the side effects are due to IL-12-induced IFNγ[25]. Thus, we tested if CBD fusion can decrease the amount of IFNγ in circulation in tumour-bearing mice. Serum IFNγ peaked on day 2 after treatment (Fig. 4a, left). CBD fusion significantly decreased systemic IFNγ levels across a broad range of doses (Fig. 4a, right). Notably, 50 μg of CBD-IL-12 (IL-12 molar basis) induced similar levels of serum IFNγ as did 10 μg of unmodified IL-12.

To further characterize the toxicity induced by cytokine treatment, we performed blood chemistry analysis on day 3 after treatment in tumour-bearing animals. Alanine

aminotransferase (ALT), a liver damage marker, is upregulated in patients treated with rhIL-12[14]. In our mouse model, serum ALT activity peaked 3 days after administration of IL-12 (Fig. 4b, left). In accord with our systemic IFNγ measurements, ALT activity levels were also reduced upon CBD fusion at doses of 10 μg and 25 μg (Fig. 4b, right). We also found that upon treatment with unmodified IL-12, but not CBD-IL-12, amylase and lipase levels were significantly elevated, suggesting reduced pancreatic damage (Supplementary Fig. 5a,b). Total serum protein levels were significantly decreased in IL-12-treated mice, indicating potential liver and kidney disorder, whereas this was not observed in the CBD-IL-12-treated cohort (Supplementary Fig. 5c). No significant changes in total bilirubin, creatinine and blood urea nitrogen levels were detected at this time point (Supplementary Fig. 5d–f). We did not observe tissue damage based on histology sections of lungs and kidneys (Supplementary Fig. 5g). CBD-IL-12 did not induce body weight loss upon treatment (Supplementary Fig. 5h). We found that the toxicity of CBD-IL-12, as indicated by serum IFNγ and ALT activity, was diminished in tumour-free animals as well (Fig. 4c,d), likely due to much shorter serum half-life of CBD-IL-12[17, 26] and slightly decreased bioactivity. Together, these data suggest that systemic toxicity of IL-12 is markedly reduced by CBD fusion.

CBD-IL-12 triggers activation of innate and adaptive immunity in a metastatic model

The advantage of CBD-IL-12 is accumulating in the tumour matrix after systemic administration, enabling treatment of both primary and metastatic tumours, including tumours in inaccessible tissues. We, thus, compared the antitumor efficacy of IL-12 and CBD-IL-12 in a B16F10 experimental lung metastasis model. 8 days after i.v. injection of B16F10 cells, metastatic nodules were visible in the lungs (Supplementary Fig. 6). After treatment with IL-12 or equimolar CBD-IL-12 on day 8, lungs were harvested on day 17 for quantification of metastatic burden. A single injection of CBD-IL-12 reduced the metastatic burden ~2-fold compared with unmodified IL-12 (Fig. 5a, Supplementary Fig. 6). We then investigated the immune cell infiltrates upon CBD-IL-12 therapy using flow cytometry. CBD-IL-12 treatment significantly increased the numbers of total T cells and $CD8^+$ T cells and decreased the frequency of regulatory T cells (Tregs) within $CD45^+$ cells compared to unmodified IL-12 (Supplementary Fig. 7a, Fig. 5b,c). Furthermore, the percentage of effector-memory $CD8^+$ T cells was significantly increased in the CBD-IL-12-treated group (Fig. 5d). The ratio of effector $CD8^+$ T cells to Tregs, an indicator of successful immunotherapy, was significantly elevated in the lungs of CBD-IL-12-treated mice (Fig. 5e). Although the total number of $CD4^+$ T cells was similar across the groups, the proportion of effector $CD4^+$ T cells was enriched in the CBD-IL-12-treated group (Supplementary Fig. 7b,c). We did not observe any differences in NK cells (Supplementary Fig. 7d) at this time point.

IL-12 plays a key role in activating the antigen presentation pathways of professional APCs through IFNγ-dependent mechanisms[27]. Treatment with CBD-IL-12 significantly increased the numbers of dendritic cells (DCs) (Fig. 5f), including cross-presenting migratory $CD103^+$ DCs (Fig. 5g) and $CD11b^+$ DCs (Fig. 5h). Furthermore, treatment with CBD-IL-12 led to an increase in the fraction of proinflammatory $CD80^+MHCII^+$ macrophages within total macrophages (Fig. 5i)[28,29]. Despite similar numbers of lung-infiltrating B

cells, phenotypically these cells were more proinflammatory in the CBD-IL-12 group, as they expressed significantly higher levels of MHCII and CD86 (Supplementary Fig. 7e, f). Collectively, the enhanced antitumor efficacy of CBD-IL-12 in a lung metastasis model indicates that our matrix-binding technology can be applied effectively to small, disseminated nodules, in addition to primary tumours, evoking a multifaceted immune reaction.

To determine which cell subtypes play important roles in reduced metastatic burden in this model, we conducted a correlation analysis using the data from the flow cytometry analysis and tumour burden in individual animals (Supplementary Fig. 8). Antitumor efficacy correlated with higher levels of total T cell infiltration, $CD8^+$ T cell infiltration and decreased numbers of Tregs (Supplementary Fig. 8a–c). Decreased metastatic burden did not correlate with increased numbers of lung-infiltrating NK cells (Supplementary Fig. 8d). Effector $CD8^+$ T cell-to-Treg ratio correlated strongly with diminished metastatic burden (Supplementary Fig. 8e). The total number of DCs and $CD103^+$ DCs, but not $CD11b^+$ DCs, correlated with less tumour burden (Supplementary Fig. 8f–h). Mice that had a higher proportion of $CD80^+MHCII^+$ macrophages had reduced metastatic burden, whereas an increased fraction of $CD86^+MHCII^+$ B cells did not correlate with improved antitumor activity (Supplementary Fig. 8i,j).

CBD-IL-12 synergizes with CPI therapy and elicits an antigen-specific immune response

CPI therapy has revolutionized the treatment of melanoma patients, yet the majority of patients cannot achieve durable responses upon CPI immunotherapy. B16F10 melanoma responds poorly to CPI therapy[30], likely due to impaired T cell infiltration and antigen presentation. Therefore, we examined if CBD-IL-12 can synergize with CPI therapy to treat large, established B16F10 tumours. Mice bearing day 9 tumours that sized around 120 mm^3 were treated twice with either PBS, CPI (α-CTLA-4 + α-PD-1), CBD-IL-12, or CBD-IL-12 + CPI (Fig. 6a,b). As expected, CPI alone had little effect on the growth of B16F10 tumours. Although CBD-IL-12 alone initially induced tumour regression, no curative responses were observed in these more established tumours, in contrast to our observation in the less established (~60 mm^3) tumours. CBD-IL-12 in combination with CPI, on the other hand, elicited a more long-lasting antitumor response, resulting in 7 CR out of 12 treated mice (58%).

Our combination immunotherapy did not involve any antigen-specific approaches, such as antitumor antibodies (e.g., TA99[31]) or vaccines comprising melanoma specific antigens (e.g., Trp1, Trp2, gp100), yet it resulted in regression of large B16F10 tumours. We hypothesized that mice whose B16F10 tumours were completely eradicated by CBD-IL-12 + CPI therapy developed a strong, antigen-specific immunological memory against melanoma antigens. To test this, we performed antigen restimulation of splenocytes from these mice. On day 60 post B16F10 challenge, splenocytes were isolated from CBD-IL-12 + CPI-treated survivor mice and stimulated with several B16F10 antigens *in vitro.* Besides common B16F10 antigens (Trp1, Trp2 and gp100), we included recently reported B16F10 neoantigens[32], kif18b and cps3fl, as well as melanocyte protein (pMel) and even B16F10 exosomes to further diversify the antigenic repertoire. After splenocyte culture in the

presence of the indicated antigens, supernatants were analysed for IFNγ and IL-2 secretion by ELISA (Supplementary Fig. 9,10). Our results demonstrate that CBD-IL-12 + CPI immunotherapy generated a broad antigen-specific response. For instance, we observed notable IFNγ responses from Trp2- and pMel-stimulated splenocytes (Supplementary Fig. 9c,d), and IL-2 responses from Trp1- and B16F10 exosome-stimulated splenocytes (Supplementary Fig. 10b,g).

We then assessed the efficacy of CBD-IL-12 + CPI in the autochthonous genetically engineered $Braf^{V600E}/PTEN^{fl/fl}$ melanoma model[33], which is partially responsive to CPI therapy[34]. CBD-IL-12 + CPI combination therapy elicited a robust control of established $Braf^{V600E}/PTEN^{fl/fl}$ melanoma growth, highlighting its strong efficacy in an induced autochthonous tumour model (Fig. 6c). On day 50 post tamoxifen application, mice were bled for immune profiling of circulating $CD8^+$ T cells (Fig. 6d–f). Mice treated with CBD-IL-12 + CPI combination experienced a 2-fold increase in circulating $CD8^+$ T cells compared to CPI treatment alone within the $CD3^+$ compartment (Fig. 6d). Nearly 60% of circulating $CD8^+$ T cells were effector cells (Fig. 6e). $CD8^+CD44^+$ T cells expressed high levels of PD-1 (Fig. 6f), indicating that these T cells are antigen-experienced, suggesting tumour reactivity[35]. We further tested the efficacy of our combination therapy in an immune-desert, $Braf^{V600E}/PTEN^{fl/fl}/\beta Cat^{STA}$ melanoma, which overexpresses β-catenin, rendering the tumour resistant to CPI therapy[36]. In this autochthonous model, combination of CBD-IL-12 and CPI resulted in strong antitumor control (Fig. 6g) and 3-fold more $CD8^+$ T cell infiltration into the tumour compared to CPI alone. Together, these results demonstrate that the combination of CBD-IL-12 with CPI is highly effective in both transplantable and cold, autochthonous tumour models, eliciting an effective, antigen-specific immune response.

Discussion

Immunotherapy has already shifted the paradigm of cancer treatment, yet improvement of the response rate and reduction of irAE frequency remains a major challenge[37], driving exploration of other approaches. For example, in murine models, complete remission of large established tumours treated with the combination of antitumor cell antibody, IL-2, α-PD-1, and vaccination (AIPV) has been recently reported[38]. While effective, this method restricts generality, in that tumour cell type-specific therapeutics (the antibody and vaccine antigen components) are needed. Thus, development of alternative therapies that are tumour type-agnostic and well-tolerated are being sought.

IL-12 is an attractive cytokine for activating multiple pathways of immunity. CBD-IL-12 efficiently accumulated in the tumour upon i.v. administration, resulting in increased and sustained production of intratumoral IFNγ. Elevated levels of intratumoral IFNγ accompanied by decreased systemic IFNγ suggests tumour-specific immune activation guided by CBD fusion. Prolonged induction of intratumoral IFNγ results in activation of APCs, a key step in the priming of antitumor immunity, leading to strong $CD8^+$ T cell responses[39]. This explains the durable antitumor response of CBD-IL-12 compared to unmodified IL-12. In the B16F10 melanoma model, CBD-IL-12 was much more effective than equimolar CBD-IL-2, our variant of another cytokine being explored in immunotherapy[12].

CBD-IL-12 treatment recruited $CD8^+$ T cells into EMT6 tumours, likely due to chemokine upregulation upon intratumoral IFNγ induction[40], turning an immune-excluded tumour into an inflamed one. Because T cell recruitment is a critical challenge for immunotherapy, this suggests CBD-IL-12 can synergize with other immunotherapies. Indeed, we showed that a strong synergy exists between CBD-IL-12 and CPI therapy. This highlights the possibility to improve CPI therapy in the clinic by combination with CBD-IL-12, as means to recruit immune cells into poorly inflamed tumours.

The CBD-based tumour targeting approach relies on accessible collagen in the tumour matrix and subsequent retention of the CBD-comprising agent in the tumour stroma. Exposed collagen around the blood vessels is a result of defective vasculature formation, a phenomenon that has been observed in human cancers[41]. We explored the targeting capability of CBD fusions in multiple tumour models with varying degrees of leakiness and inflammation. For example, primary B16F10 melanoma grows very rapidly, meaning that the vasculature in this model could potentially be very disordered. To explore response in smaller, metastatic lesions, where vascular remodelling is slower, we examined the pulmonary metastatic B16F10 model, in which CBD-IL-12 was also more efficacious than the untargeted IL-12. We also showed favourable efficacy in two autochthonous models, where tumour growth is even slower, and one displays very low inflammation, boding well for the translatability of our matrix-targeting approach to human patients.

Clinical trials using systemic rhIL-12 were terminated due to intolerable irAEs[14, 42]. The main toxicities observed in these clinical trials were cytokine storm (particularly, high levels of serum IFNγ) and grade 3 hepatotoxicity, defined as more than 5-fold increase of ALT over normal levels[43]. In our study, we demonstrate that CBD fusion to IL-12 significantly decreases serum IFNγ and hepatic and pancreatic damage markers and does not cause any apparent histological damage in the kidneys and lungs. This, again, suggests that CBD-IL-12 activates antitumor immunity rather than autoimmunity in healthy tissues. The beneficial effect on toxicity is not only due to sequestration of CBD-IL-12 in the tumour, since CBD fusion to IL-12 also decreased toxicity in non-tumour-bearing mice. Decreased toxicity in tumour-free mice can be explained by slightly reduced EC_{50} and the substantially shorter serum half-life of CBD-IL-12 compared to IL-12. The faster systemic clearance may be due to binding to matrix in the liver and kidney, in which the endothelium is fenestrated, as we have previously observed[12]. In a clinical setting, this may be highly advantageous, since the toxicity benefit of CBD fusion does not fully depend on tumour burden. This may also be beneficial from a drug development point of view, as preclinical evaluation of toxicity is usually conducted in healthy animals. Thus, the accelerated clearance from the blood, paired with the prolonged pharmacodynamic effect in the tumour (as evidenced by prolonged intratumoral IFNγ elevation) is particularly attractive. Our toxicity studies demonstrate that CBD-IL-12 therapy is better tolerated than therapy with untargeted IL-12, which is encouraging for its clinical translation.

For clinical translation, one additional advantage is that CBD-IL-12 can target tumour stroma after i.v. injection, which is a common route for many clinical anticancer drugs. Other injection routes, such as intratumoral injection, have been applied to rIL-12[11, 44] and plasmids encoding IL-12[45]. However, systemic injection of drugs is convenient, does

not cause injection-site reactions and can target not only superficial tumours, but also inaccessible/metastatic tumours. Interestingly, we observed that i.v.-injected CBD-IL-12 was more efficacious than p.t.-administered CBD-IL-12. This may reflect more favourable accumulation of CBD-IL-12 within the tumour stroma by vascular distribution than along a needle track and associated interstitial dispersion[46] and thus greater availability of CBD-IL-12 to the immune cells.

IL-12 has also been engineered for systemic administration as a fusion protein with antibodies against components that are specifically expressed within the tumour microenvironment, such as those targeting the ED-B domain of tumour fibronectin[47] and necrosis-derived DNA[48]. These strategies are being tested in the clinic, showing promise for employing active targeting approaches[49]. A potential shortcoming in using antibody-fused cytokines, though, is that they can generate anti-drug antibody responses[50]. By our design of CBD-IL-12, a potential advantage lies in the use of a CBD protein that naturally exists in the blood, here the A3 domain from VWF, limiting the possibility of immune system recognition. The only possible immunogenic component in our design is the $(G_3S)_2$ linker connecting CBD to each of the subunits.

In conclusion, we have utilized a molecular engineering approach to improve IL-12 therapy in aspects of both efficacy and safety. CBD-IL-12 therapy induced a prolonged elevation in intratumoral IFNγ while demonstrating lower systemic IFNγ, compared to treatment with unmodified IL-12. CBD-IL-12 monotherapy eradicated immunologically cold tumours in the EMT6 breast cancer model by a single injection. Combination therapy with CPI induced regression of large and aggressive B16F10 tumours, stabilized the growth of the genetically-engineered $Braf^{V600E}/PTEN^{fl/fl}$ melanoma, and caused T cell infiltration in CPI-unresponsive $Braf^{V600E}/PTEN^{fl/fl}/\beta Cat^{STA}$ melanoma. CBD-IL-12 therapy is not antigen-specific, but capable of antigen-specific response induction. CBD-IL-12 therapy is simple and highly efficacious, holding a high translational promise.

Methods

Mice and cancer cell lines

8 to 12-week-old C57Bl/6 female mice were purchased from Charles River Laboratory. 8 to 12-week-old Balb/c female mice were purchased from Jackson Laboratory. B16F10 and EMT6 breast cancer cell lines were obtained from ATCC and cultured according to instructions. *Tyr:Cre-ER$^+$/LSL-Braf^{V600E}/Pten$^{fl/fl}$* and *Tyr:Cre-ER$^+$/LSL-Braf^{V600E}/PTEN$^{fl/fl}$/βCat^{STA}* mice, ages 6 to 12 weeks were bred at the animal facility of the University of Chicago. All animal experiments performed in this work were approved by the Institutional Animal Care and Use Committee of the University of Chicago. Cell lines were routinely checked for mycoplasma contamination.

Production and purification of recombinant IL-12 and CBD-IL-12

For the production of wild-type IL-12, optimized sequences encoding murine p35 and p40 subunits were synthesized and subcloned into mammalian expression vector pcDNA3.1(+) by Genscript. A sequence encoding $(His)_6$ was added to the N-terminus of the p35 subunit

to allow affinity-based protein purification. For the production of CBD-IL-12, sequence encoding the CBD protein (A3 domain of VWF[12]) was fused to the N-terminus of the murine p35 subunit via $(GGGS)_2$ linker and to the C-terminus of the murine p40 subunit via $(GGGS)_2$ linker. $(His)_6$ tag was added to the N-terminus of the CBD-p35 subunit. Sequences encoding CBD-p35 and p40-CBD were subcloned into mammalian expression vector pcDNA3.1(+) by Genscript. Suspension-adapted HEK-293F were maintained in serum-free Free Style 293 Expression Medium (Gibco). On the day of transfection, cells were inoculated into fresh medium at a concentration of 1×10^6 cells/mL. 500 μg/L p35 (or CBD-p35) plasmid DNA, 500 μg/L p40 (or p40-CBD) plasmid DNA were mixed with 2 mg/L linear 25 kDa polyethyleneimine (Polysciences) and co-transfected in OptiPRO SFM medium (4% final volume). After 7 days of culture, supernatants were harvested, and purification was performed as described before[12, 51]. Purified proteins were tested for endotoxin via HEK-Blue TLR4 reporter cell line and endotoxin levels were confirmed to be less than 0.01 EU/mL. Protein purity was assessed by SDS-PAGE as described previously[12, 52]. Protein concentration was determined through absorbance at 280 nm using NanoDrop (Thermo Scientific).

MALDI-TOF MS analysis of IL-12 and CBD-IL-12

IL-12 and CBD-IL-12 were analysed by MALDI-TOF MS using Bruker Ultraflextreme MALDI-TOF/TOF instrument. All spectra were collected with acquisition software Bruker flexControl™ and processed with analysis software Bruker flexAnalysis™. First, a saturated solution of the matrix, α-cyano-4-hydroxycinnamic acid (Sigma-Aldrich), was prepared in 50:50 (v/v) acetonitrile:(1% TFA in water). The analyte in PBS (5 μL, 0.1 mg/mL) and the matrix solution (25 μL) were then mixed and the mixture centrifuged for 2 min (myFUGE by Benchmark). The supernatant (1 μL) was then deposited on the MTP 384 ground steel target plate. The drop was dried rapidly in a nitrogen gas flow, which resulted in the formation of uniform sample/matrix coprecipitate. All samples were analysed using high mass linear positive mode method with 5000 laser shots at a laser intensity of 75%. The measurements were externally calibrated at three points with a mix of carbonic anhydrase, phosphorylase B, and bovine serum albumin.

Analysis of STAT4 phosphorylation by flow cytometry

Mouse $CD8^+$ T cells were purified from spleens of C57BL/6 mice using EasySep mouse $CD8^+$ T cell isolation kit (Stem Cell). Purified $CD8^+$ T cells (10^6 cells/mL) were activated in six-well plates precoated with 2 μg/mL α-CD3 (clone 17A2, Bioxcell) and supplemented with soluble 5 μg/mL α-CD28 (clone 37.51, BioLegend) and 30 ng/mL mouse IL-2 (Peprotech) for 3 days. Culture medium was IMDM (Gibco) containing 10% heat-inactivated FBS, 1% Penicillin/Streptomycin and 50 μM 2-mercaptoethanol (Sigma Aldrich). After 3 days of culture, activated $CD8^+$ T cells were rested for 6 hrs in fresh culture medium and were transferred into 96-well plates (50,000 cells/well). Indicated amounts of IL-12 or CBD-IL-12 were applied to $CD8^+$ T cells for 20 min at 37 °C to induce STAT4 phosphorylation. Cells were fixed immediately using BD Phosflow Lyse/Fix buffer for 10 min at 37 °C and then permeabilized with BD Phosflow Perm Buffer III for 30 min on ice. Cells were stained with Alexa Fluor (AF) 647-conjugated antibody against pSTAT4 (clone 38, BD) recognizing phosphorylation of Tyr693. Staining was performed

for 1 hr at room temperature (RT) in the dark. Cells were acquired on BD LSR and data were analysed using FlowJo (Treestar). Mean Fluorescence Intensity (MFI) of $pSTAT4^+$ population was plotted against cytokine concentration. Dose-response curve was fitted using Prism (v8, GraphPad).

Splenocyte activation test

To assess *in vitro* bioactivity of produced IL-12 and CBD-IL-12, splenocytes were isolated from C57Bl/6 mice, plated in 96-well plates at 5×10^5 cells/well. CBD-IL-12 or IL-12 were added to the wells at indicated concentrations. 48 h later, cell supernatants were assayed using IFNγ ELISA (Invitrogen). Culture medium was RPMI (Gibco) supplemented with 10% heat inactivated FBS, 1% Penicillin/Streptomycin, 5 mM HEPES (Gibco) and 10 ng/mL mouse IL-2 (Peprotech). Dose-response curve was fitted using Prism (v8, GraphPad).

Surface Plasmon Resonance (SPR) against collagen I and III

SPR measurements were made with a Biacore X100 SPR system (GE Healthcare). Collagen I or collagen III (EMD Millipore) was immobilized via amine coupling on a CM5 chip (GE Healthcare) for ~1000 resonance units (RU) according to the manufacturer's instructions. CBD-IL-12 was flowed for 90 sec (for collagen I) and for 30 sec (for collagen III) at increasing concentrations in the running buffer at 30 μL/min. The sensor chip was regenerated with 50 mM NaOH for every cycle. Specific binding of CBD-IL-12 to collagen was calculated automatically using the response to a non-functionalized channel as a reference. Binding curves were fitted using BIAevaluation software (GE Healthcare). Binding results were fitted with Langmuir binding kinetics (1:1 binding with drifting baseline Rmax local).

Detection of IL-12 and CBD-IL-12 binding to human melanoma cryosections

Human melanoma cryosections were purchased from OriGene Technologies. Cryosections were first blocked with 2% BSA in PBS-T at RT. 50 μg of CBD-IL-12 (IL-12 molar basis) or IL-12 were added to sections and incubated for 2 hr at RT. Tissues were then stained with the following primary antibodies: rabbit anti-human collagen I antibody (Abcam, ab34710), mouse anti-human CD31 antibody (Abcam, ab119339) and rat anti-mouse IL-12p70 antibody (from mouse IL-12p70 ELISA kit, Invitrogen). Tissues were then stained with the following fluorescently-labelled secondary antibodies: Alexa 594-labeled donkey anti-rat IgG (Jackson Immunoresearch Labs, 712586153), Alexa 488-labeled donkey anti-mouse IgG (Jackson Immunoresearch Labs, 715546151), and Alexa 647-labeled donkey anti-rabbit IgG (Jackson Immunoresearch Labs, 711605152). Secondary antibody staining was performed for 1 hr. Sections were then covered with Prolong Gold Antifade Mountant containing DAPI (Thermo Fisher) and sealed with a coverslip. Microscopy was performed using IX73 microscope (Olympus) and images were processed using ImageJ software (NIH).

Antitumor efficacy of IL-12 and CBD-IL-12

For the primary tumour model of B16F10 melanoma, 5×10^5 B16F10 cells were inoculated intradermally on the back of the female C57Bl/6 mouse in 30 μL sterile PBS. For the EMT6

mammary carcinoma model, 5×10^5 EMT6 cells were injected into the left mammary fat pad of female Balb/c mice in 30 μL sterile PBS. For the secondary challenge of EMT6 carcinoma, 5×10^5 EMT6 cells were injected in the opposite mammary fat pad, 3 months after the primary challenge. Dose and schedule of the cytokines and antibodies are described in the figure legends. For i.v. routes, compounds were injected in 100 μL volume. For p.t. injection, compounds were administered in 30 μL volume. The volume of the tumour was calculated using the following formula: (height) × (width) × (thickness) × (π/6). Mice were sacrificed when the tumour volume reached 1000 mm^3 and/or based on humane end-point criteria.

Tumour accumulation in EMT6-bearing mice and biodistribution in tumour-free mice

IL-12 or CBD-IL-12 protein was fluorescently labelled using DyLight 650 NHS ester (Thermo Fisher), and unreacted dye was removed by a Zebaspin spin column (Thermo Fisher) according to the manufacturer's instruction. For tumour accumulation experiments, total of 5×10^5 EMT6 cells re-suspended in 50 μL of PBS were injected subcutaneously into the mammary fat pad on the right side of each Balb/c mouse. When the tumour reached approximately 500 mm^3, 25 μg DyLight 650 labelled IL-12 or 25 μg (16.5 μg IL-12 basis) DyLight 650-labeled CBD-IL-12 was injected i.v. 1 hr after injection, mice were sacrificed and tumours were extracted and imaged with the Xenogen IVIS Imaging System 100 (Xenogen) under the following conditions: f/stop: 2; optical filter excitation 640 nm; emission 670 nm; exposure time: 0.5 sec; small binning. The protein amount in each tumour was calculated based on a standard dilution series of IL-12 or CBD-IL-12 labelled with DyLight650 and normalized to the weight of the tumour. Biodistribution experiment in tumour-free mice was performed similarly.

Pharmacokinetics of IL-12 and CBD-IL-12

Naïve C57Bl/6 mice received doses of 25 μg of IL-12 or 25 μg of CBD-IL-12 (IL-12 equimolar basis) i.v. (n = 3/group). 15 μL of blood was collected from the tail 10 min, 30 min, 60 min and 240 min after injection in EDTA-containing heparinized tubes. Plasma was separated and concentrations of IL-12 and CBD-IL-12 were measured by IL-12p70 ELISA (Invitrogen). Plasma was diluted 5000 times for 10, 30 and 60 min, and 1000 times for 240 min. In-house-produced IL-12 and CBD-IL-12 served as the standards for the ELISA. No endogenous IL-12 could be detected from PBS-injected mice. Plasma half-life was estimated assuming one phase decay model (v8, GraphPad Prism).

Serum IFNγ and blood chemistry analysis

For assessment of serum IFNγ, mice were treated with either IL-12 or molar equivalent of CBD-IL-12. On indicated days, blood was collected in protein low-binding tubes (Eppendorf). Blood was allowed to clot overnight at 4°C. The next day, serum was obtained by centrifugation at 4000 × g for 10 min. IFNγ ELISA (Invitrogen) was performed on the sera (18x dilution) according to manufacturer's instructions. No endogenous IFNγ could be detected at this dilution from PBS-treated animals. Alanine aminotransferase (ALT) assay (Sigma-Aldrich) was performed using sera (4x dilution), according to manufacturer's instructions. Serum amylase, lipase, total protein, total bilirubin, creatinine and blood urea nitrogen were determined using Vet Axcel blood chemistry analyser (Alfa Wasserman).

Histological assessment of lungs and kidney

5×10^5 B16F10 cells were inoculated intradermally on the back of the female C57Bl/6 mouse in 30 μL sterile PBS. Mice received doses of 25 μg of IL-12 or 25 μg of CBD-IL-12 (IL-12 equimolar basis) i.v. 7 days after inoculation. 3 days after cytokine treatment, lungs and kidneys were collected and fixed with 2% paraformaldehyde. After paraffin embedding, blocks were cut into 5 μm sections, followed by staining with hematoxylin and eosin. Slides were imaged by EVOS FL Auto (Life Technologies). Slides were blindly assessed for tissue damage.

Histological analysis of EMT6 tumours

5×10^5 EMT6 cells were injected into left mammary fat pad of Balb/c mice. 7 days later, mice were treated with either PBS or CBD-IL-12 (25 μg IL-12 basis). On day 10, tumors were collected and fixed with 2% paraformaldehyde. After paraffin embedding, blocks were cut into 5 μm sections, followed by staining with hematoxylin and eosin. After deparaffinization and rehydration, tissue sections were treated with target retrieval solution (S1699, DAKO) and heated in steamer for 20 min at temperature >95 C°. Tissue sections were incubated with anti-mouse CD8 antibody (clone 4SM15, eBioscience) for 1 hr incubation at RT in a humidity chamber. Following TBS wash, the tissue sections were incubated with biotinylated anti-rat IgG (10 μg/mL, Vector laboratories) for 30 min at RT. The antigen-antibody binding was detected by Elite kit (PK-6100, Vector Laboratories) and DAB (DAKO, K3468) system. Slides were imaged by EVOS FL Auto (Life Technologies).

Intratumoral IFNγ kinetics and intratumoral cytokines/chemokines

Mice bearing day 7 B16F10 tumours were treated with either IL-12 or CBD-IL-12 and sacrificed on day 9, 10 and 11. Tumours were collected, snap frozen in liquid nitrogen and stored at −80°C. Tumours were then homogenized in Tissue Protein Extraction buffer (T-PER, Thermo Fisher). Protease inhibitor tablets (Roche) were added to the T-PER buffer. Tumours were placed in Lysing Matrix D tubes (MP Bio). Homogenization was performed using Fast-Prep tissue homogenizer (MP Bio). IFNγ was quantified using IFNγ ELISA (Invitrogen) and normalized by total protein content. Total protein content was measured using Pierce BCA Protein Assay (Thermo Fisher). Luminex assay was performed using Milliplex assay (Millipore Sigma) according to manufacturer's instructions.

Analysis of *in vivo* IFNγ-producing cells in B16F10 melanoma

Protocol for identification of *in vivo* IFNγ-producing immune cells has been described previously[24]. 5×10^5 B16F10 cells were inoculated intradermally on the back of the female C57Bl/6 mouse in 30 μL sterile PBS. 6 days after tumour implantation, mice were treated with either PBS or CBD-IL-12. On day 10, mice were given 250 μg of brefeldin A (BFA) (Sigma Aldrich) in 500 μL via intraperitoneal (i.p.) injection. 5 hr after BFA injection, tumours were harvested and digested for 30 min at 37 °C. Digestion medium was DMEM (Gibco) supplemented with 5% FBS, 2.0 mg/mL Collagenase D (Sigma), 20 μg/mL DNAse I (Worthington Biochemical), 1.2 mM $CaCl_2$ and 10 μg/mL BFA. Single-cell suspensions were prepared using a 70 μm cell strainer (Fisher). 20 mg of tumour was plated per well. For antibodies against surface targets, the staining was done in PBS with

2% FBS. For intracellular targets, staining was performed according to the manufacturer's protocols (00–5523-00, Thermo Fisher Scientific). Following anti-mouse antibodies were used: CD45 Allophycocyanine-Cy7 (APC-Cy7) (clone 30-F11, BioLegend), CD3ε BUV395 (clone 145–2C11, BD), CD4 Brilliant Violet (BV) 785 (clone RM4–5, BioLegend), CD8α BV510 (clone 53–6.7, BioLegend), Foxp3 PE (clone MF23, BD), CD11c PE-Cy7 (clone N418, BioLegend), NK1.1 BV605 (clone PK136, BioLegend), MHCII PerCP-Cy5.5 (clone, M5/114.15.2, BioLegend), CD11b BUV737 (clone M1/70, BD), IFNγ APC (clone XMG1.2, BioLegend), F4/80 AF488 (clone BM8, BioLegend), CD103 eFluor 450 (clone 2E7, ThermoFisher). Cell viability was determined using the fixable viability dye eFluor 455UV dye (65–0868-14, eBioscience). Cells were acquired on BD LSR and data were analysed using FlowJo (Treestar).

Pulmonary metastatic model of B16F10 melanoma

For the pulmonary metastasis model of B16F10 melanoma, female C57Bl/6 mice were injected i.v. with 5×10^5 B16F10 cells in 100 μL volume. Mice received treatment 8 days after the challenge. On day 17, the lungs were perfused with PBS and imaged for quantification of the metastatic burden. To assess the metastatic burden, we quantified the total area of B16 nodules using ImageJ (NIH) and normalized it by the total area of the lung.

Generation of single-cell suspension from the lungs for flow cytometry

Mice were perfused through the left ventricle of the heart with 10 mL of PBS. The lung lobes were then isolated and digested. Briefly, the lobes were cut into small pieces with a scissor and then digested in 5 mL DMEM (Gibco) with 5% FBS, 1 mg/mL Collagenase IV (Worthington Biochemical), 3.3 mg/mL Collagenase D (Sigma), 20 μg/mL DNAse I (Worthington Biochemical) and 1.2 mM $CaCl_2$ for 60 min at 37 °C on a shaker. After quenching the media with 5 mM EDTA (Gibco), single-cell suspensions were prepared using a 70 μm cell strainer (Fisher). Finally, red blood cells were lysed with 1 mL ACK lysing buffer (Gibco) for 90 sec and neutralized with 10 mL DMEM media with 5% FBS.

Analysis of immune infiltrates in the pulmonary metastatic model of B16F10 melanoma

Single cell suspensions were counted after digestion and 2×10^6 live cells/well were plated for staining. For antibodies against surface targets, the staining was done in PBS with 2% FBS. For intracellular targets, staining was performed according to the manufacturer's protocols (00–5523-00, Thermo Fisher Scientific). The following anti-mouse antibodies were used for flow cytometry: CD45 APC-Cy7 (clone 30-F11, BioLegend), CD3ε BUV395 (clone 145–2C11, BD), Foxp3 AF647 (clone MF23, BD), CD8α AF488 (clone 53–6.7, BioLegend), CD4 BV785 (clone RM4–5, BioLegend), CD25 PE (clone PC61, BioLegend), CD44 PerCP-Cy5.5 (clone IM7, BioLegend), CD62L BUV737 (clone MEL-14, BD), NK1.1 BV421 (clone PK136, BD), CD103 PE (clone 2E7, BioLegend), CD86 BV510 (clone GL-1, BioLegend), F4/80 APC (clone A3–1, AbD Serotec), CD11c PE-Cy7 (clone N418, BioLegend), CD11b BV786 (clone M1/70, BD), CD80 BUV737 (clone 16–10A1, BD Biosciences), CD19 BUV395 (clone 1D3, BD), Ly6G FITC (clone 1A8-Ly6g, eBioscience), Ly6C BV605 (clone HK1.4, BioLegend), MHCII PerCP-Cy5.5 (clone, M5/114.15.2, BioLegend), CD8α PacBlue (53–6.7, BioLegend). Cell viability was determined using the fixable viability dye eFluor 455UV dye (65–0868-14, eBioscience).

Combination therapy with checkpoint inhibitors (CPI)

In combination therapy studies, 5×10^5 B16F10 cells in 30 μL were injected intradermally on the back of the female C57Bl/6 mice. PBS, 25 μg CBD-IL-12 (IL-12 molar eq.) and CPI were administered on days 9 and 14 post B16F10 challenge. CPI stands for a combination of 100 μg α-CTLA-4 (9H10, Bioxcell) and 100 μg α-PD-1 (29F.1A12, Bioxcell). CPI was administered via i.p. injection. CBD-IL-12 was administered via i.v. injection.

Induction of autochthonous $Braf^{V600E}/PTEN^{fl/fl}$ and $Braf^{V600E}/PTEN^{fl/fl}/\beta Cat^{STA}$ tumour models, analysis of circulating T cells and immunofluorescence

8–12-week old *Tyr:Cre-ER*$^+$*/LSL-Braf*^{V600E}*/Pten*$^{fl/fl}$ mice were shaved on the back and 5 μL of 4-OH-tamoxifen was applied topically. 25 days after tamoxifen application, mice were divided into two groups. CPI-treated cohort received α-PD-1 and α-CTLA-4 i.p., 100 μg each. CBD-IL-12 + CPI-treated mice received 25 μg of CBD-IL-12 (IL-12 molar eq.) via i.v. injection and indicated amount of CPI via i.p. injection. The same treatment was given on days 30, 39 and 44 for a total of 4 treatments. Tumour size was measured using calipers and the tumour volume was calculated according to the following formula: (width) × (height) × (thickness) × π/4. For the analysis of circulating $CD8^+$ T cells from $Braf^{V600E}/PTEN^{-/-}$ mice, mice were bled on day 50 post tamoxifen induction. Red blood cells were lysed with ACK lysing buffer (Gibco). Cell viability was assessed with the Fixable Viability Dye eFluor 455 UV from eBioscience. Antibodies used for flow cytometry included: CD45 APC-Cy7 (clone 30-F11, BioLegend), CD3 FITC (clone 145–2C11, BioLegend), CD8α PE-Cy7 (clone 53–6.7, BioLegend), CD62L BUV737 (clone MEL-14, BD), CD44 PerCP-Cy5.5 (clone IM7, BD) and PD-1 BV605 (clone 29F.1A12, BioLegend). Induction of melanoma in *Tyr:Cre-ER*$^+$*/LSL-Braf*^{V600E}*/Pten*$^{fl/fl}$*/βCat*^{STA} mice was performed similarly[53]. 25 days after tamoxifen application, mice received either CPI or CBD-IL-12 + CPI (dosed as mentioned above). Treatment was given every 5 days until day 45. On day 50, tumours were excised and fixed in formalin-free zinc fixative (BD) for 2 days. Tumours were placed in 15% sucrose (in TBS) for 2 days followed by 30% sucrose (in TBS) for additional 2 days. Tumours were frozen and 7-μm sections were obtained. Cryosections were blocked with 0.5% casein in TB for 1 hr at RT. Sections were then incubated with rat anti-mouse CD8α (clone 53–6.7, BD) for 2 hr at RT. Slides were incubated with AF594-conjugated goat anti-rat (Jackson ImmunoResearch Labs) for 1 hr at RT. Sections were then covered with Prolong Gold Antifade Mountant containing DAPI (Thermo Fisher) and sealed with a coverslip. Microscopy was performed using IX73 microscope (Olympus). Image processing and $CD8^+$ T cell counting was performed using ImageJ software (NIH).

Antigen restimulation of splenocytes

Spleens were harvested from mice that cured B16F10 melanoma by CBD-IL-12 + CPI immunotherapy or from age-matched naïve mice. Splenocytes were plated at a density of 10^6/well in 200 μL of DMEM (Gibco) supplemented with 10% heat-inactivated FBS and 1% Penicillin/Streptomycin. Peptides used in restimulation assays were synthesized by Genscript and the sequences were as follows: gp100 (KVPRNQDWL), Trp1 (CRPGWRGAACNQKI), Trp2 (SVYDFFVWL), kif18b (PSKPSFQEFVDWEN**N**VSPELNSTDQPFLP, mutation K739N),

cps3fl (EFKHIKAFDRTFA**N**NPGPMVVFATPGML, mutation D314N). Bold amino acid represents the mutation. pMel (SILV) protein was purchased from Abnova. Peptides were used at a concentration of 2 μg/mL, pMel protein was used at 5 μg/mL. B16 exosomes were produced in-house and used at 50 μg/mL. All samples were run in duplicate. Cells were cultured for 72 hr. Cell culture supernatants were collected and immediately assayed for IL-2 and IFNγ by ELISA (Invitrogen).

Statistical analysis

Statistical analysis between groups was performed using Prism software (v8, GraphPad). For multiple comparisons of means, one-way ANOVA followed by Tukey's post hoc test was used if the data were found to be parametric by Brown-Forsythe test. For nonparametric data with multiple groups, Kruskal-Wallis test followed by Dunn's multiple comparison test was used. For comparison between two groups, a two-tailed Student's t-test with Welch's correction was used. For nonparametric data with two groups (determined by F test), Mann-Whitney test was used. Survival curves between two groups were analysed using the log-rank (Mantel-Cox) test.

Data availability

The main data supporting the results in this study are available within the paper and its Supplementary Information. All data generated in this study, including source data and the data used to make the figures, are available from figshare with the identifier 10.6084/m9.figshare.11971371.

Reporting summary.

Further information on research design is available in the Nature Research Reporting Summary linked to this article.

Supplementary Material

Refer to Web version on PubMed Central for supplementary material.

Acknowledgements

We would like to thank T. Gajewski (University of Chicago) for sharing *Tyr:Cre-ER^{+}/LSL-Braf^{V600E}/PTEN$^{fl/fl}$* and *Tyr:Cre-ER^{+}/LSL-Braf^{V600E}/PTEN$^{fl/fl}$/βCat^{STA}* mice, Ani Solanki for assistance with tail vain injections, Suzana Gomes for assistance with experiments, Terri Li for assistance with histology analysis, the Human Tissue Resource Center of the University of Chicago for assistance with organ sectioning and D. Leclerc (University of Chicago Flow Cytometry Core) for assistance with Luminex assay.

References

1. Larkin J. et al. Combined Nivolumab and Ipilimumab or Monotherapy in Untreated Melanoma. The New England journal of medicine 373, 23–34 (2015). [PubMed: 26027431]
2. Sharma P. & Allison JP The future of immune checkpoint therapy. Science 348, 56–61 (2015). [PubMed: 25838373]
3. Rosenberg SA, Yang JC & Restifo NP Cancer immunotherapy: moving beyond current vaccines. Nature medicine 10, 909–915 (2004).
4. Langrish CL et al. IL-12 and IL-23: master regulators of innate and adaptive immunity. Immunol Rev 202, 96–105 (2004). [PubMed: 15546388]

5. McHeyzer-Williams MG et al. Antigen-specific immunity. Immunologic Research 22, 223–236 (2000). [PubMed: 11339358]
6. Fallarino F, Ashikari A, Boon T. & Gajewski TF Antigen-specific regression of established tumors induced by active immunization with irradiated IL-12- but not B7–1-transfected tumor cells. Int Immunol 9, 1259–1269 (1997). [PubMed: 9310829]
7. Rogge L. et al. Selective expression of an interleukin-12 receptor component by human T helper 1 cells. The Journal of experimental medicine 185, 825–831 (1997). [PubMed: 9120388]
8. Tugues S. et al. New insights into IL-12-mediated tumor suppression. Cell Death Differ 22, 237–246 (2015). [PubMed: 25190142]
9. Lasek W, Zagozdzon R. & Jakobisiak M. Interleukin 12: still a promising candidate for tumor immunotherapy? Cancer immunology, immunotherapy : CII 63, 419–435 (2014). [PubMed: 24514955]
10. Kerkar SP et al. IL-12 triggers a programmatic change in dysfunctional myeloid-derived cells within mouse tumors. The Journal of clinical investigation 121, 4746–4757 (2011). [PubMed: 22056381]
11. Momin N. et al. Anchoring of intratumorally administered cytokines to collagen safely potentiates systemic cancer immunotherapy. Sci Transl Med 11 (2019).
12. Ishihara J. et al. Targeted antibody and cytokine cancer immunotherapies through collagen affinity. Sci Transl Med 11 (2019).
13. Bekaii-Saab TS et al. A phase I trial of paclitaxel and trastuzumab in combination with interleukin-12 in patients with HER2/neu-expressing malignancies. Mol Cancer Ther 8, 2983–2991 (2009). [PubMed: 19887543]
14. Atkins MB et al. Phase I evaluation of intravenous recombinant human interleukin 12 in patients with advanced malignancies. Clinical cancer research : an official journal of the American Association for Cancer Research 3, 409–417 (1997). [PubMed: 9815699]
15. Gollob JA et al. Phase I trial of concurrent twice-weekly recombinant human interleukin-12 plus low-dose IL-2 in patients with melanoma or renal cell carcinoma. J Clin Oncol 21, 2564–2573 (2003). [PubMed: 12829677]
16. Mariathasan S. et al. TGFbeta attenuates tumour response to PD-L1 blockade by contributing to exclusion of T cells. Nature 554, 544–548 (2018). [PubMed: 29443960]
17. Zhang Y, Li N, Suh H. & Irvine DJ Nanoparticle anchoring targets immune agonists to tumors enabling anti-cancer immunity without systemic toxicity. Nat Commun 9, 6 (2018). [PubMed: 29295974]
18. Joyce JA & Fearon DT T cell exclusion, immune privilege, and the tumor microenvironment. Science 348, 74–80 (2015). [PubMed: 25838376]
19. Gollob JA et al. Phase I trial of twice-weekly intravenous interleukin 12 in patients with metastatic renal cell cancer or malignant melanoma: ability to maintain IFN-gamma induction is associated with clinical response. Clinical cancer research : an official journal of the American Association for Cancer Research 6, 1678–1692 (2000). [PubMed: 10815886]
20. Ayers M. et al. IFN-gamma-related mRNA profile predicts clinical response to PD-1 blockade. The Journal of clinical investigation 127, 2930–2940 (2017). [PubMed: 28650338]
21. Spranger S, Dai D, Horton B. & Gajewski TF Tumor-Residing Batf3 Dendritic Cells Are Required for Effector T Cell Trafficking and Adoptive T Cell Therapy. Cancer cell 31, 711–723.e714 (2017). [PubMed: 28486109]
22. Wang LL et al. CXC-chemokine-ligand-10 gene therapy efficiently inhibits the growth of cervical carcinoma on the basis of its anti-angiogenic and antiviral activity. Biotechnology and applied biochemistry 53, 209–216 (2009). [PubMed: 19257857]
23. Ghiringhelli F. et al. Activation of the NLRP3 inflammasome in dendritic cells induces IL-1beta-dependent adaptive immunity against tumors. Nature medicine 15, 1170–1178 (2009).
24. Liu F. & Whitton JL Cutting edge: re-evaluating the in vivo cytokine responses of CD8+ T cells during primary and secondary viral infections. Journal of immunology (Baltimore, Md. : 1950) 174, 5936–5940 (2005). [PubMed: 15879085]
25. Ryffel B. Interleukin-12: role of interferon-gamma in IL-12 adverse effects. Clinical immunology and immunopathology 83, 18–20 (1997). [PubMed: 9073529]

26. Neri D. Antibody-Cytokine Fusions: Versatile Products for the Modulation of Anticancer Immunity. Cancer Immunol Res 7, 348–354 (2019). [PubMed: 30824549]
27. Zhou F. Molecular mechanisms of IFN-gamma to up-regulate MHC class I antigen processing and presentation. Int Rev Immunol 28, 239–260 (2009). [PubMed: 19811323]
28. Clatza A, Bonifaz LC, Vignali DA & Moreno J. CD40-induced aggregation of MHC class II and CD80 on the cell surface leads to an early enhancement in antigen presentation. Journal of immunology (Baltimore, Md. : 1950) 171, 6478–6487 (2003). [PubMed: 14662847]
29. Ho PC et al. Immune-based antitumor effects of BRAF inhibitors rely on signaling by CD40L and IFNgamma. Cancer research 74, 3205–3217 (2014). [PubMed: 24736544]
30. Pan D. et al. A major chromatin regulator determines resistance of tumor cells to T cell-mediated killing. Science 359, 770–775 (2018). [PubMed: 29301958]
31. Boross P. et al. Anti-tumor activity of human IgG1 anti-gp75 TA99 mAb against B16F10 melanoma in human FcgammaRI transgenic mice. Immunol Lett 160, 151–157 (2014). [PubMed: 24613852]
32. Castle JC et al. Exploiting the mutanome for tumor vaccination. Cancer research 72, 1081–1091 (2012). [PubMed: 22237626]
33. Dankort D. et al. Braf(V600E) cooperates with Pten loss to induce metastatic melanoma. Nat Genet 41, 544–552 (2009). [PubMed: 19282848]
34. Ishihara J. et al. Matrix-binding checkpoint immunotherapies enhance antitumor efficacy and reduce adverse events. Sci Transl Med 9 (2017).
35. Gros A. et al. PD-1 identifies the patient-specific CD8(+) tumor-reactive repertoire infiltrating human tumors. The Journal of clinical investigation 124, 2246–2259 (2014). [PubMed: 24667641]
36. Spranger S, Bao R. & Gajewski TF Melanoma-intrinsic beta-catenin signalling prevents anti-tumour immunity. Nature 523, 231–235 (2015). [PubMed: 25970248]
37. Drake CG, Lipson EJ & Brahmer JR Breathing new life into immunotherapy: review of melanoma, lung and kidney cancer. Nat Rev Clin Oncol 11, 24–37 (2014). [PubMed: 24247168]
38. Moynihan KD et al. Eradication of large established tumors in mice by combination immunotherapy that engages innate and adaptive immune responses. Nature medicine 22, 1402–1410 (2016).
39. Garris CS et al. Successful Anti-PD-1 Cancer Immunotherapy Requires T Cell-Dendritic Cell Crosstalk Involving the Cytokines IFN-gamma and IL-12. Immunity 49, 1148–1161.e1147 (2018). [PubMed: 30552023]
40. Coughlin CM et al. Tumor cell responses to IFNgamma affect tumorigenicity and response to IL-12 therapy and antiangiogenesis. Immunity 9, 25–34 (1998). [PubMed: 9697833]
41. Nagy JA, Chang SH, Dvorak AM & Dvorak HF Why are tumour blood vessels abnormal and why is it important to know? Br J Cancer 100, 865–869 (2009). [PubMed: 19240721]
42. Leonard JP et al. Effects of single-dose interleukin-12 exposure on interleukin-12-associated toxicity and interferon-gamma production. Blood 90, 2541–2548 (1997). [PubMed: 9326219]
43. Grigorian A. & O'Brien CB Hepatotoxicity Secondary to Chemotherapy. J Clin Transl Hepatol 2, 95–102 (2014). [PubMed: 26357620]
44. van Herpen CM et al. Intratumoral recombinant human interleukin-12 administration in head and neck squamous cell carcinoma patients modifies locoregional lymph node architecture and induces natural killer cell infiltration in the primary tumor. Clinical cancer research : an official journal of the American Association for Cancer Research 11, 1899–1909 (2005). [PubMed: 15756016]
45. Mahvi DM et al. Intratumoral injection of IL-12 plasmid DNA--results of a phase I/IB clinical trial. Cancer Gene Ther 14, 717–723 (2007). [PubMed: 17557109]
46. Swartz MA & Lund AW Lymphatic and interstitial flow in the tumour microenvironment: linking mechanobiology with immunity. Nat Rev Cancer 12, 210–219 (2012). [PubMed: 22362216]
47. Halin C. et al. Enhancement of the antitumor activity of interleukin-12 by targeted delivery to neovasculature. Nat Biotechnol 20, 264–269 (2002). [PubMed: 11875427]
48. Fallon J. et al. The immunocytokine NHS-IL12 as a potential cancer therapeutic. Oncotarget 5, 1869–1884 (2014). [PubMed: 24681847]

49. Strauss J. et al. First-in-Human Phase I Trial of a Tumor-Targeted Cytokine (NHS-IL12) in Subjects with Metastatic Solid Tumors. Clinical cancer research : an official journal of the American Association for Cancer Research 25, 99–109 (2019). [PubMed: 30131389]

50. Hank JA et al. Immunogenicity of the Hu14.18-IL2 Immunocytokine Molecule in Adults With Melanoma and Children With Neuroblastoma. Clinical Cancer Research 15, 5923–5930 (2009). [PubMed: 19737959]

51. Williford JM et al. Recruitment of CD103(+) dendritic cells via tumor-targeted chemokine delivery enhances efficacy of checkpoint inhibitor immunotherapy. Sci Adv 5, eaay1357 (2019).

52. Sasaki K. et al. Engineered collagen-binding serum albumin as a drug conjugate carrier for cancer therapy. Sci Adv 5, eaaw6081 (2019).

53. Ishihara J. et al. Improving Efficacy and Safety of Agonistic Anti-CD40 Antibody Through Extracellular Matrix Affinity. Mol Cancer Ther 17, 2399–2411 (2018). [PubMed: 30097487]

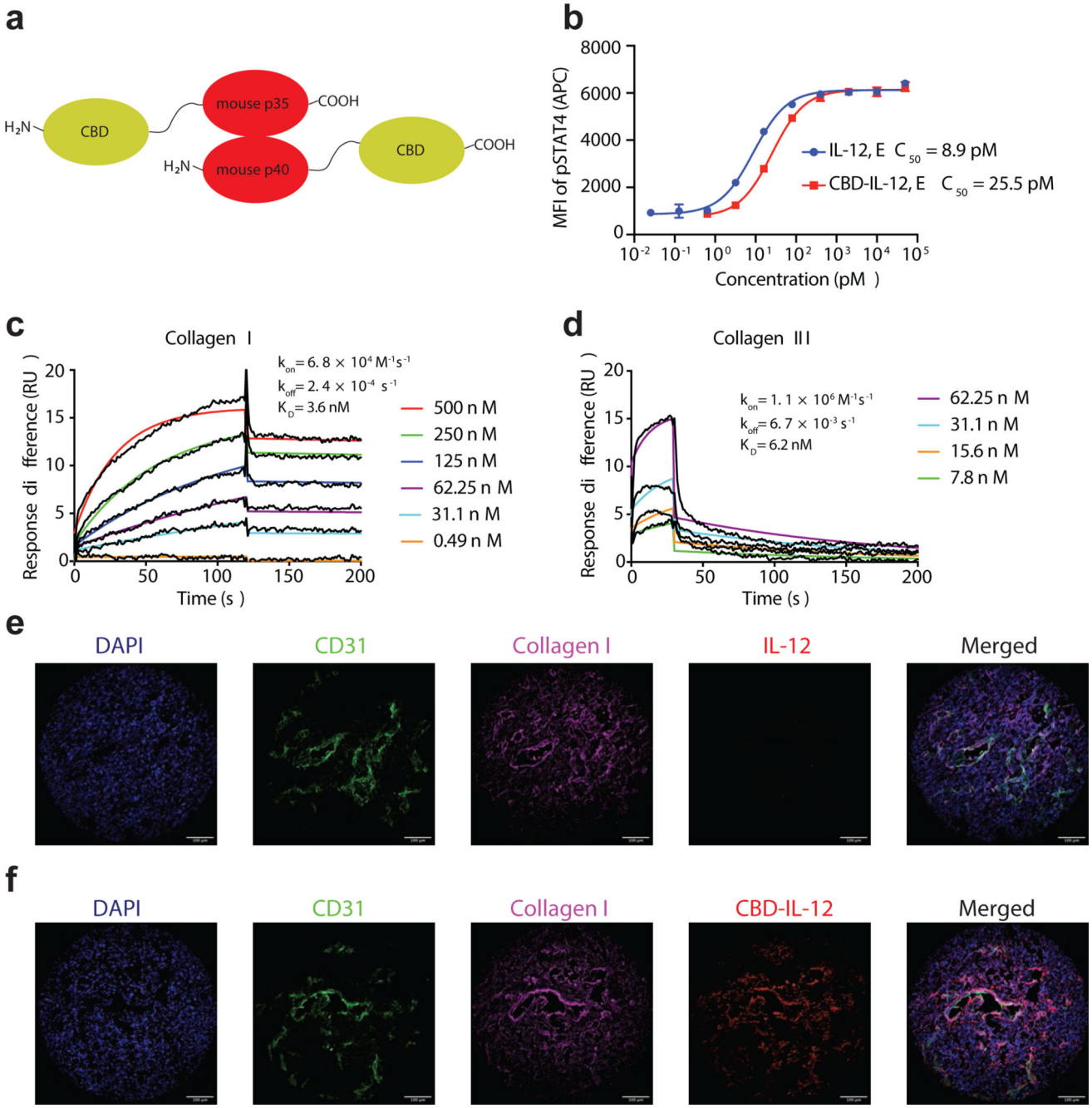

Fig. 1 |. CBD-IL-12 binds to collagen with high affinity while retaining bioactivity.

a, Schematic illustrating the fusion sites of the von Willebrand factor A3 CBD to murine p35 and p40 subunits. CBD was fused to each of the subunits via a $(GGGS)_2$ linker. **b,** Dose-response relationship of phosphorylated STAT4 with IL-12 and CBD-IL-12 in preactivated primary mouse $CD8^+$ T cells (n = 3, mean ± SD). **c,d,** Affinity (K_D values are shown) of CBD-IL-12 against collagen I (**c**) and collagen III (**d**) as measured by SPR. CBD-IL-12 was flowed over the chips at indicated concentrations. Curves represent the specific responses (in resonance units, RU) to CBD-IL-12. Experimental curves were fitted with 1:1

Langmuir model. Dissociation constants (K_D) and rate constants (k_{on} and k_{off}) determined from the fitted curves are shown. **e,f,** Binding of unmodified IL-12 (**e**) or CBD-IL-12 (**f**) to human melanoma cryosections was imaged by fluorescence microscopy. Scale bars, 100 μm. Experiments were performed twice (**b,c,d,e,f)**, with similar results. Representative data are shown.

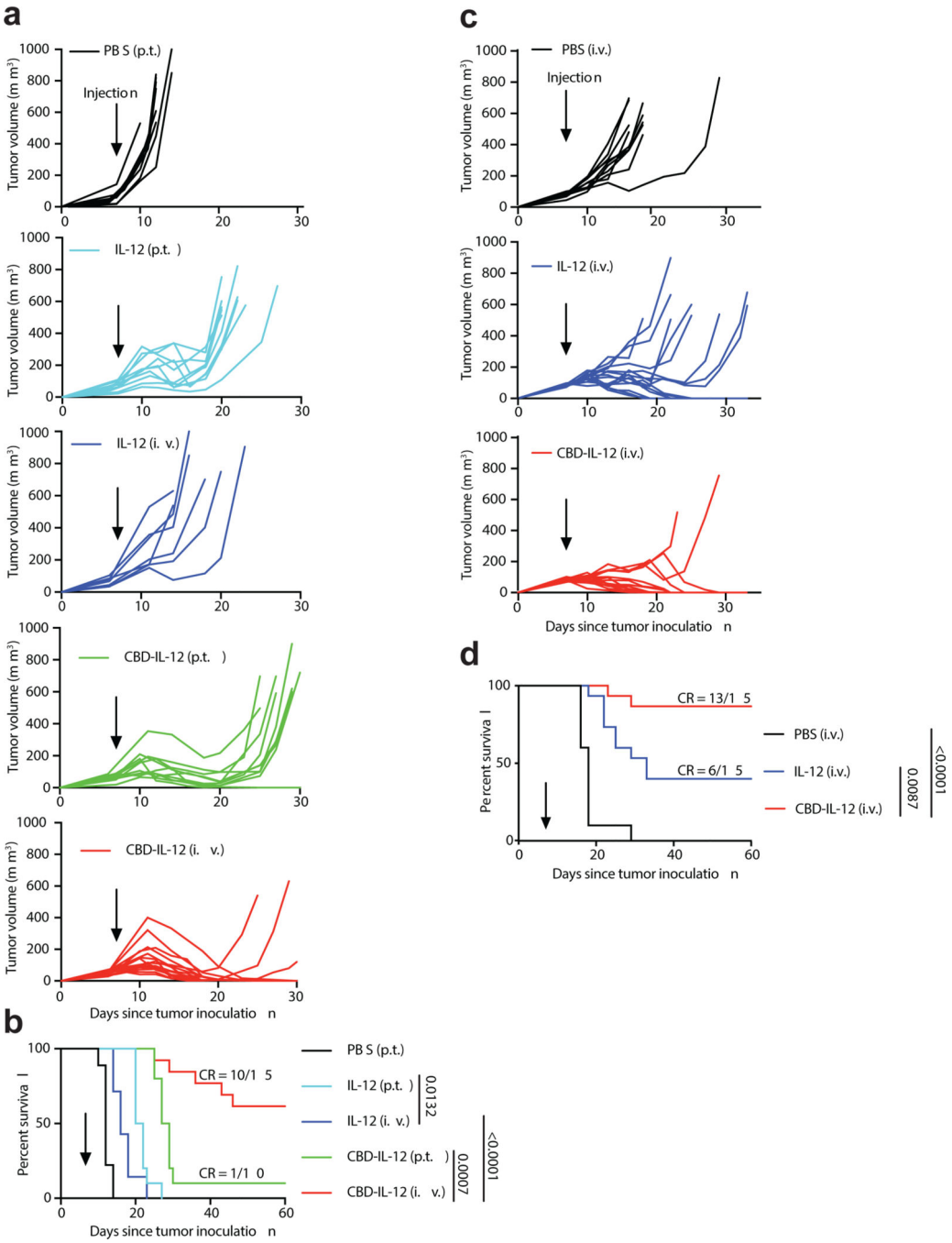

Fig. 2 |. CBD-IL-12 induces regression of B16F10 melanoma and EMT6 mammary carcinoma. **a,b,** 5×10^5 B16F10 melanoma cells were inoculated intradermally on back skin and mice were treated with either PBS (p.t., n = 9), 25 μg IL-12 (p.t., n = 10), 25 μg IL-12 (i.v., n = 7), equimolar CBD-IL-12 (p.t., n = 10), or equimolar CBD-IL-12 (i.v., n = 15) once on day 7. Individual tumour curves (**a**) and survival curves (**b**) are shown. **c,d,** 5×10^5 EMT6 mammary carcinoma cells were inoculated into the left mammary fat pad and mice were treated i.v. with either PBS (n = 7), 25 μg IL-12 (n = 15) or equimolar CBD-IL-12 (n = 15) once on day 7. Individual tumour curves (**c**) and survival curves (**d**) are shown. Data are

compiled from two independent experiments. Statistical analyses were done using log-rank (Mantel-Cox) test.

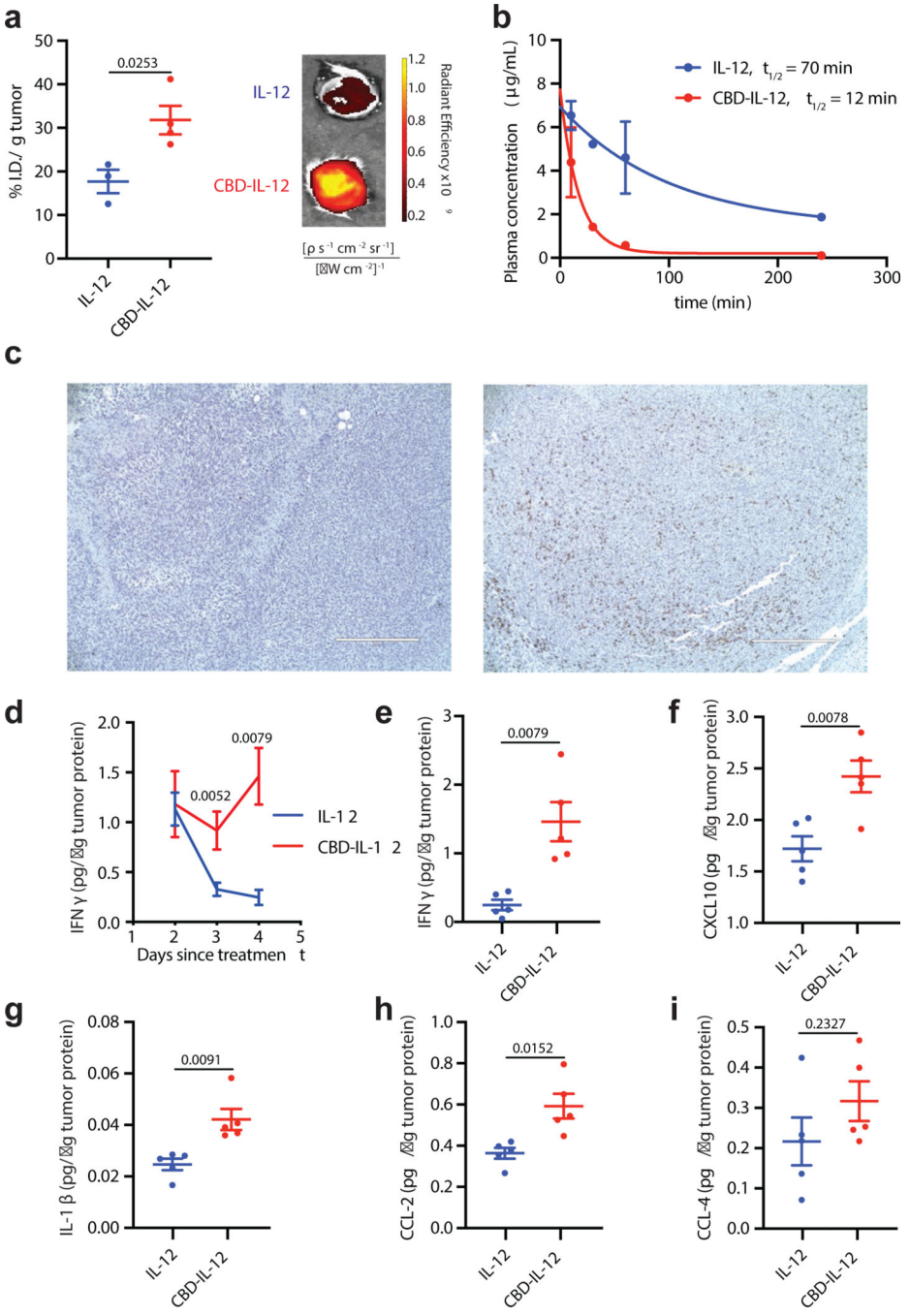

Fig. 3 |. CBD-IL-12 induces intratumoral inflammation by rapidly localizing into the tumour.
a, Mice bearing EMT6 tumours were injected i.v. with 25 µg of DyLight 650-labeled IL-12 (n = 3) or CBD-IL-12 (n = 4). Fluorescence intensity in each tumour was measured using IVIS 1 hr post injection and normalized to the weight of the tumour. **b,** Naïve C57BL/6 mice were administered 25 µg IL-12 (n = 3) or equimolar CBD-IL-12 (n = 3) via i.v. injection. Blood was collected at the indicated time points, plasma was separated and analysed for IL-12p70 concentration via ELISA. **c,** Mice bearing established EMT6 tumours were injected i.v. with either PBS (left, n = 3) or 25 µg CBD-IL-12 (IL-12 molar eq., right,

n = 3) and 3 days after injection, tumours were, fixed and stained with H&E and anti-mouse CD8 (brown). Scale bar = 400 μm. **d,** B16F10 melanoma-bearing mice were treated with either 25 μg IL-12 or equimolar CBD-IL-12 i.v. once on day 7 and tumours were harvested 2, 3 and 4 days after treatment. Tumours were homogenized for protein extraction and IFNγ levels were quantified using ELISA and normalized by total tumour protein content. For day 2, n = 9. For day 3, n = 10. For day 4, n = 5. **f-i,** Luminex assay was performed on day 4 tumour lysates and analysed for indicated cytokines/chemokines (n = 5). Data are mean ± SEM. Experiments in **a,b,c** were performed twice, with similar results. Representative data are shown. In **d,** data were compiled from two independent experiments. Luminex assay was performed once on independent biological samples. Statistical analyses were done using unpaired, two-tailed t-test with Welch correction for **a,f,g,h** and two-tailed Mann-Whitney test for **d,e,i** due to nonparametric data.

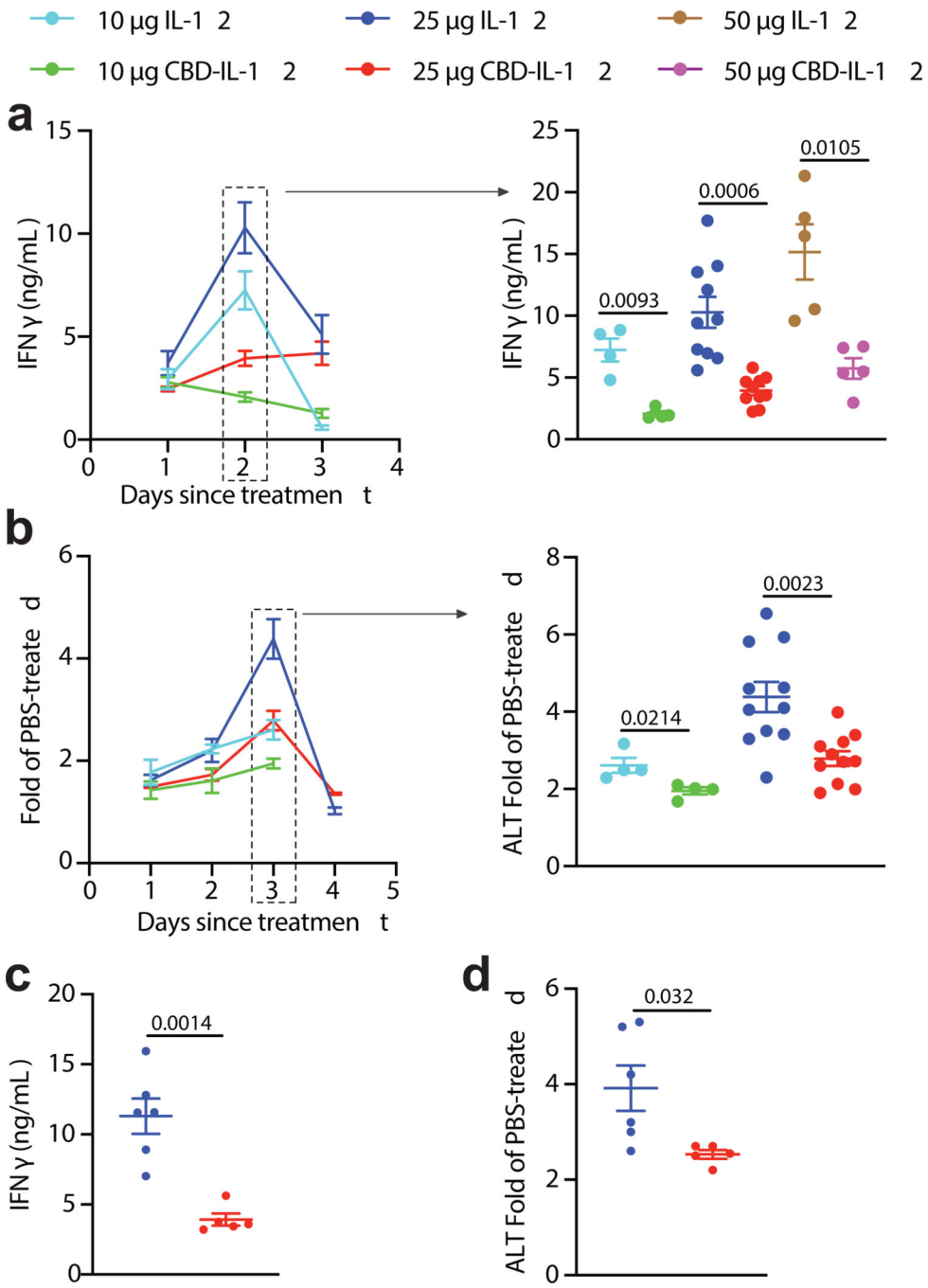

Fig. 4 |. CBD-IL-12 minimizes irAEs in tumour-bearing and non-tumour-bearing mice.
a,b, 7 days before cytokine treatment, 5×10^5 B16F10 melanoma cells were inoculated and mice were treated i.v. with either 10, 25, 50 μg IL-12 or with either 10, 25 or 50 μg CBD-IL-12 (IL-12 molar eq.) once on day 0. **a,** Kinetics of IFNγ levels (left) and day 2 comparison (right) in the serum are shown. **b,** Kinetics of serum ALT activity (left) and day 3 comparison (right) are shown. Data are represented as fold of PBS-treated. For 10 μg groups, n = 4. For 25 μg groups, n = 11. For 50 μg groups, n = 5. **c,d,** Naïve C57BL/6 mice received either 25 μg IL-12 or 25 μg CBD-IL-12 (IL-12 molar eq.) once on day 0

and bled on days 2 and 3 for IFNγ and ALT activity measurements, respectively. n = 5 per group. Data are mean ± SEM. Data are compiled from three independent experiments. Statistical analyses between two groups were done using unpaired, two-tailed t-test with Welch correction.

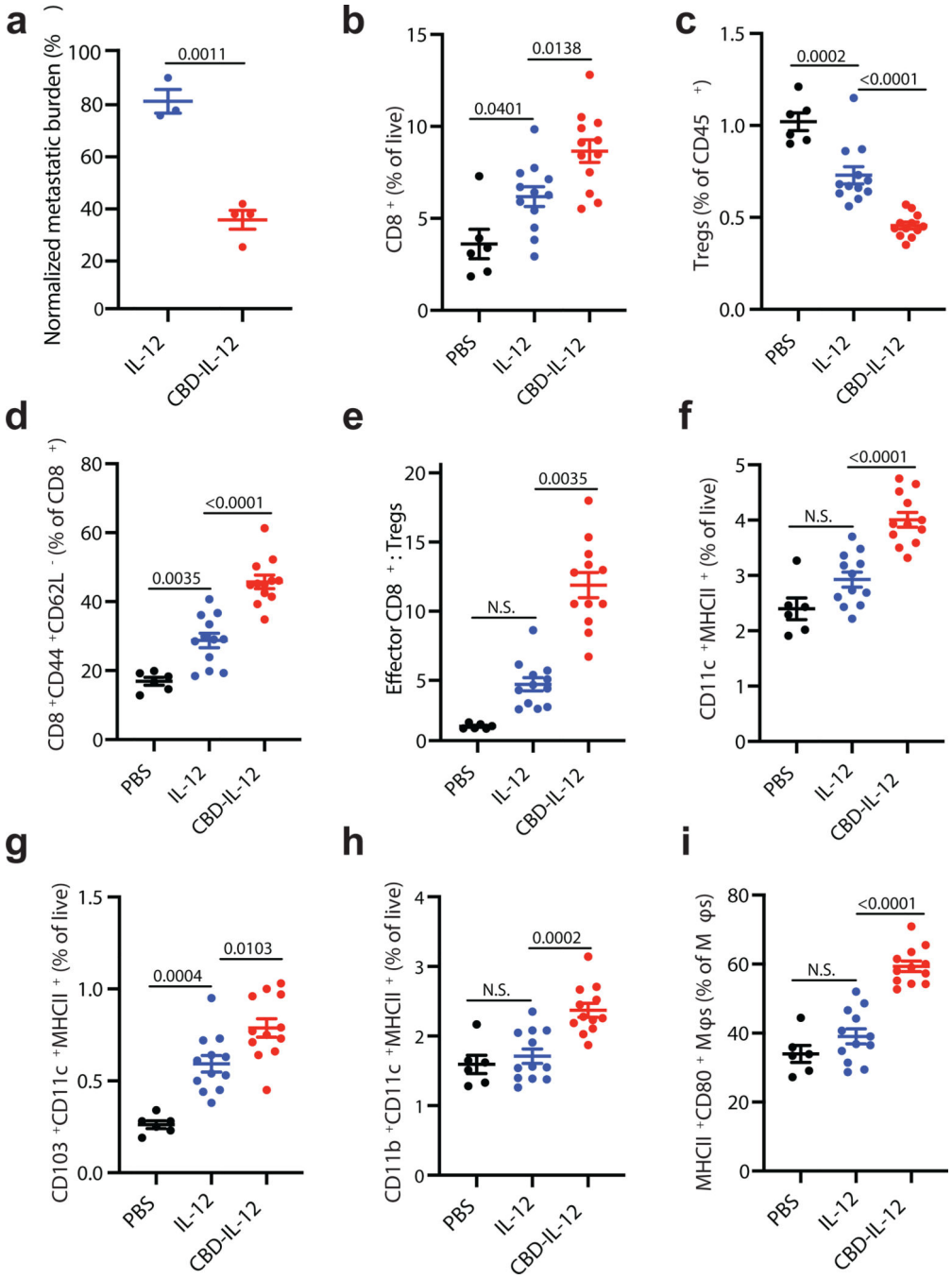

Fig. 5 |. CBD-IL-12 decreases metastatic tumour burden by triggering activation of innate and adaptive compartments of the immune system in the pulmonary metastatic model of B16F10 melanoma.

a, 5×10^5 B16F10 cells were injected i.v. on day 0. Mice were treated with either 25 μg IL-12 (n = 3) or with equimolar CBD-IL-12 (n = 4) i.v. once on day 8 and sacrificed on day 17. Metastatic burden was quantified using ImageJ software and normalized by total area of the lung. **b-i,** 2.5×10^5 B16F10 cells were injected i.v. on day 0. Mice were treated with either PBS (n = 6), 25 μg IL-12 (n = 12) or with equimolar CBD-IL-12 (n = 12) i.v. once on day 9 and lungs were collected on day 18. 2×10^6 live cells/well were plated for flow

cytometric analysis. **b,** Percentages of $CD3^+CD8^+$ T cells within live cells. **c,** Frequency of $CD3^+CD4^+CD25^+Foxp3^+$ Tregs within lung-infiltrating immune cells (% of $CD45^+$). **d,** Frequency of $CD3^+CD8^+CD44^+CD62L^-$ effector $CD8^+$ T cells within total $CD8^+$ T cells. **e,** Ratio of effector $CD8^+$ T cells to Tregs. **f-h,** Percentages of DCs ($CD11c^+MHCII^+F4/80^-$) (**f**), $CD103^+$ DCs (**g**), and $CD11b^+$ DCs (**h**) within live cells. **i,** Frequency of $MHCII^+CD80^+$ macrophages within total macrophages (defined as $CD11b^+F4/80^+$). Lines represent mean ± SEM. Antitumor efficacy experiment (**a**) was performed twice, with similar results. Flow analysis was performed once on independent biological samples. Statistical analyses were done using unpaired, two-tailed t-test with Welch's correction (**a**), ordinary one-way ANOVA with Tukey's test for parametric data (**b,c,d,f,g,h,i)** and Kruskal-Wallis test followed by Dunn's multiple comparison for nonparametric data (**e**).

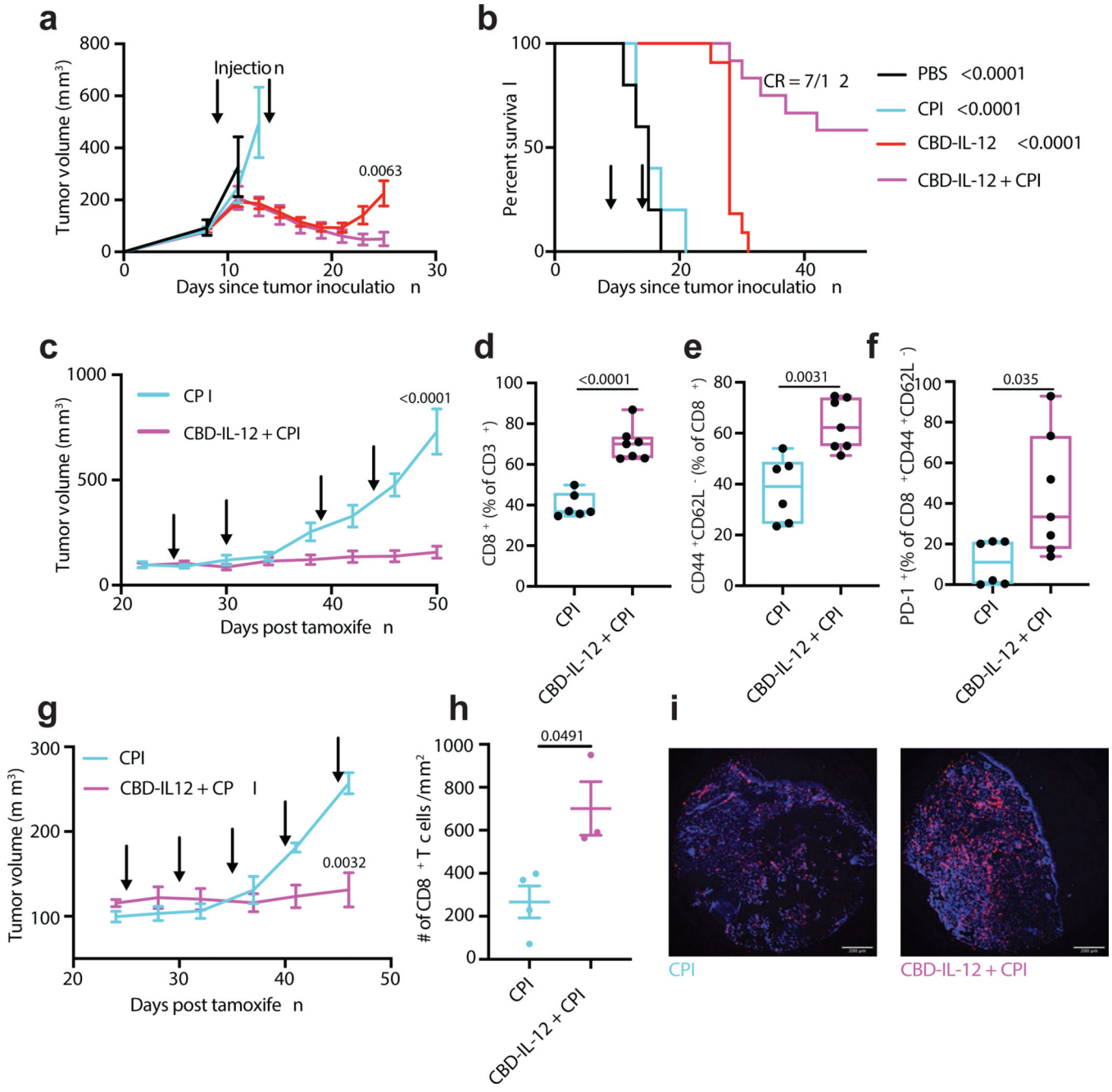

Fig. 6 |. CBD-IL-12 synergizes with CPI and elicits tumour antigen-specific response.

a,b, 5×10^5 B16F10 cells were inoculated intradermally on day 0. PBS (n = 5), α-PD-1 + α-CTLA-4 (CPI, 100 μg each; n = 5), 25 μg CBD-IL-12 (IL-12 molar eq., n = 11) or CBD-IL-12 + CPI (n = 12) were administered on days 9 and 14. CBD-IL-12 was administered i.v. and CPI was administered i.p. Tumour growth curves (**a**) and survival curves (**b**) are shown. **c-f,** *Tyr:Cre-ER*$^{+}$*/LSL-Braf*^{V600E}*/PTEN*$^{fl/fl}$ mice received 50 μg of 4-OH-tamoxifen on their back. Mice were treated with CPI (n = 6) or CBD-IL-12 + CPI (n = 7) on days 25, 30, 39 and 44 post tamoxifen application. **d-f,** On day 50, mice were bled for the analysis of circulating T cells. Box plots (median, min to max) for total $CD8^+$ T

cells (% of $CD3^+$) (**d**), effector $CD8^+$ T cells (% of $CD8^+$ T cells) (**e**), and $PD\text{-}1^+$ cells (% of effector $CD8^+$ T cells) (**f**) are shown. **g-i,** *Tyr:Cre-ER$^+$/LSL-Braf^{V600E}/PTEN$^{fl/fl}$/βCat^{STA}* mice received 50 μg of 4-OH-tamoxifen on their back. Mice were treated with CPI (n = 4) or CBD-IL-12 + CPI (n = 4) on days 25, 30, 35, 40, 45 post tamoxifen application. **h,i,** On day 50, tumours from CPI (n = 4) and CBD-IL-12 + CPI (n = 3) were excised, fixed and stained with DAPI (blue) and anti-mouse CD8 (purple). For each tumour sample, $CD8^+$ T cells were counted within two different fields and average was calculated (mean ± SEM). Representative images (**i**) are shown. Scale bars, 200 μm. Tumour curves are represented as mean ± SEM. Experiments in **a,b,** were performed twice, with similar results. $Braf^{V600E}/PTEN^{fl/fl}$ and $Braf^{V600E}/PTEN^{fl/fl}/βCat^{STA}$ experiments were performed once on distinct biological samples. Statistical analysis for **a,c,d,e,g,h** was done using unpaired, two-tailed t-test with Welch correction. For **f,** two-tailed Mann-Whitney test was applied due to nonparametric data. Statistical analysis for survival curve was done using log-rank test.